Theoretical study of high photocatalytic performance of Ag_3PO_4

Naoto Umezawa,[1,2] Ouyang Shuxin,[1,2] and Jinhua Ye[1,2,3]

[1]*Photocatalytic Materials Center, National Institute for Materials Science, Ibaraki 305-0047, Japan*

[2]*Innovative Center of Nanomaterials Science for Environment and Energy (ICNSEE), National Institute for Materials Science, Ibaraki 305-0047, Japan*

[3]*International Center for Materials Nanoarchitectonics (MANA), National Institute for Materials Science, Ibaraki 305-0044, Japan*

(Received 9 August 2010; revised manuscript received 13 October 2010; published 13 January 2011)

The recent discovery of an excellent photocatalyst, Ag_3PO_4, motivated us to clarify the origin of its high performance. Our comprehensive study using density-functional-theory-based calculations has revealed that the formation of PO_4 tetrahedral units with strong P-O bonds weakens the covalent nature of Ag-O bonds, inhibiting hybridization of Ag *d* and O *p*. This excludes the *d* character from the conduction-band minimum (CBM), leaving highly dispersive Ag *s*-Ag *s* hybrid bands. The delocalized charge distribution of the CBM results in a small effective mass of the electron, which is advantageous for the carrier transfer to surface.

DOI: 10.1103/PhysRevB.83.035202 PACS number(s): 71.20.Ps, 88.40.H−

I. INTRODUCTION

Photocatalysis has attracted enormous attention in recent years for its great potential in harvesting solar energy for environmental purification and fuel production.[1–3] Water splitting with solar light is an ideal approach for sustainable human life. Since the discovery of the Hoda-Fujishima effect of TiO_2,[4] the quest for highly efficient photocatalysts has been conduced in the past three decades. One important aspect in designing photocatalysts is to sensitize their activities under visible light. The commonly used photocatalyst TiO_2 possesses a relatively wide band gap (3.2 eV for anatase and 3.0 eV for rutile), and thus its photoabsorption spectrum is in a range of ultraviolet, which accounts for only 4% of solar light. To further accelerate photocatalytic activities, utilizing visible light, which dominates 43% of the solar light and almost 100% of indoor light, is a crucial task.

Historically, metal doping[5,6] or anion doping[7,8] into TiO_2 are the popular strategies for narrowing band gaps so as to enhance visible-light absorption. One drawback of doping is that impurity sites act as carrier recombination centers where photoexcited electrons and holes are annihilated by combing to each other before participating in chemical reactions on surface. Thus, even though visible-light absorption is increased in some cases, dramatic improvement of overall photocatalytic efficiency is not expected by means of impurity doping.

For this reason, many other materials have been extensively studied in the hope of finding desirable band structures for visible-light-sensitive photocatalysts.[9,10] Among them, silver-based oxides are found to be promising.[11–16] Ag_2O itself does not show photocatalytic activities for water splitting owing to its too small band gap [1.3 eV (Ref. 17)], causing the conduction-band minimum (CBM) or the valence-band maximum (VBM) to be energetically too low or too high with respect to the reduction or oxidation potentials of water, respectively. Combining Ag_2O with other transition-metal oxides such as Nb_2O_5 and Ta_2O_5, which possess wide band gaps compared to Ag_2O, is useful for shifting the band edges. In fact, $AgNbO_3$ is known as a visible-light-driven photocatalyst for oxygen evolution.[11] Ouyang *et al.* have reported the photocatalytic performance of $AgAlO_2$ as a pioneer case of incorporating *p*-block elements, i.e., atomic species with partially occupied *p* states as the valence, into Ag_2O.[12] The importance of *p*-block elements lies in the fact that the conduction band formed with *s* and *p* states is highly dispersive compared to that composed of *d* states, and, therefore, it is advantageous for the electron transfer.[18,19] This explains why some of the oxides with *p*-block elements such as SnO_2 and ZnO show good conductivity when doped with donor impurities.[20] Subsequent works for $AgGaO_2$,[13,14] Ag_2ZnGeO_4,[15] and $AgSbO_3$ (Ref. 16) have inferred that the *p*-block elements are actually important ingredients for silver-based photocatalysts. However, these previous works were focused on metallic elements in the *p*-block atoms, and nonmetallic species had never been incorporated into Ag_2O in the context of photocatalysis research.

Recently, our group has discovered strong oxidation power of Ag_3PO_4, with which a quantum yield of O_2 gas generation from water splitting marks nearly 90% under visible light.[21] Given the fact that most photocatalysts show a relatively poor quantum yield as low as 20%, the exceptionally high efficiency of Ag_3PO_4 is intriguing. From electrochemical measurements, the CBM of Ag_3PO_4 was found to be lower than the reduction potential of hydrogen, and it is unable to evolve H_2 from water splitting, while it has a sufficiently positive VBM with respect to the oxidation potential of water and possesses a large power of water oxidation. Thus, photoexcited electrons are not directly involved in the oxidation reaction and must be scavenged by so-called sacrificial reagents ($AgNO_3$) for continuous reaction of O_2 evolution.[21] Nevertheless, the nature of electron transfer is indirectly related to the overall photocatalytic activities through electron-hole recombination, which degrades the efficiency of photocatalysis processes. Therefore, physical properties of both carriers are important to understand the excellent performance of Ag_3PO_4. Although a first-principles calculation was carried out in the previous work, the knowledge to understand the mechanism is still insufficient.

In this article, we report our comparative study for electronic structures of Ag_3PO_4, Ag_2O, and $AgNbO_3$. In Sec. II, we address the computational details of our

density-functional-theory-based calculations for these three oxides. In Sec. III, we discuss the role of Ag s states at CBM with computational results for density of states (DOS) and band structures. Effective masses of the electron and hole are also shown in our tables. Based on the theoretical analysis, we conclude in Sec. IV that the absence of d character at the CBM contributes to realizing a small effective mass of the electron in Ag_3PO_4.

II. COMPUTATIONAL PROCEDURE

Our first-principles calculations are based on the density-functional theory within the local-density approximation (LDA). The calculations were performed using the projector augmented wave pseudopotentials as implemented in the VASP code.[22,23] The valence configurations of the pseudopotentials are $4d^{10}5s^1$ for Ag, $2s^22p^4$ for O, $3s^23p^3$ for P, and $4p^64d^45s^1$ for Nb. Both Ag_3PO_4 and Ag_2O adopt a cubic phase (space group $P\bar{4}3n$ for Ag_3PO_4 and $Pn\bar{3}m$ for Ag_2O), consisting of 16- and six-atom unit cells, respectively, while $AgNbO_3$ has a more complex structure, with an orthorhombic symmetry (space group $Pbcm$) with 40-atom unit cells. These crystal structures are depicted in Fig. 1. A silver atom is coordinated with four and two oxygen atoms in Ag_3PO_4 and Ag_2O, respectively. In $AgNbO_3$, there are two Ag sites of threefold and fourfold. We used an energy cutoff of 500 eV in the plane-wave basis-set expansion. Monkhorst-Pack k-point sets of $4\times4\times4$, $6\times6\times6$, and $4\times4\times2$ were used for Ag_3PO_4, Ag_2O, and $AgNbO_3$, respectively. The cell volume and atomic positions were relaxed until the residual forces were below 0.03 eV/Å. We have also performed LDA + U calculations[24] for Ag_3PO_4, Ag_2O, and $AgNbO_3$ in order to investigate the effects of on-site Coulomb repulsion (Hubbard U) at d states of Ag and Nb atoms, which are insufficiently described in LDA. In the case of Ag_2O, we applied $U=5.8$ eV to Ag d states, following Ref. 17. The values of U for Ag_3PO_4 and $AgNbO_3$ are not available in the literature, and thus we used two different U values determined by the following procedure. First, we estimated U for a single Ag^+ ion by subtracting atomic total energies E_{tot} of three different occupations of d states:[25] $U^{atm}(Ag^+) = [E_{tot}(d^{10}) - E_{tot}(d^9)] - [E_{tot}(d^9) - E_{tot}(d^8)] = 13.92$ eV, where the self-interaction correction was taken into account with the Perdew-Zunger-type LDA correlation energy functional.[26] By considering screening effects, we simply took 30% and 70% of U^{atm} as the values of U in bulk Ag_3PO_4 and $AgNbO_3$: $U^{(1)}(Ag) = 4.18$ eV and $U^{(2)}(Ag) = 9.75$ eV. The same procedure was taken for the Nb atom and we found that $U^{atm}(Nb^+) = 10.8$ eV, and thus $U^{(1)}(Nb) = 3.24$ eV and $U^{(2)}(Nb) = 7.56$ eV. The obtained lattice parameters from LDA and LDA + U are listed in Table I. The on-site Coulomb interaction does not significantly affect the lattice constants, and they are in good agreement with experimental data. For comparison, relaxed bond distances given by LDA for Ag_3PO_4, Ag_2O, and $AgNbO_3$ are listed in Table II with experimental values. The Ag-O distances are elongated in Ag_3PO_4 as compared to those in Ag_2O, reflecting a less covalent nature of the Ag-O bonds in Ag_3PO_4, while Ag-Ag distances are rather shortened in Ag_3PO_4, indicating the formation of metallic Ag-Ag bonds. It was also found that

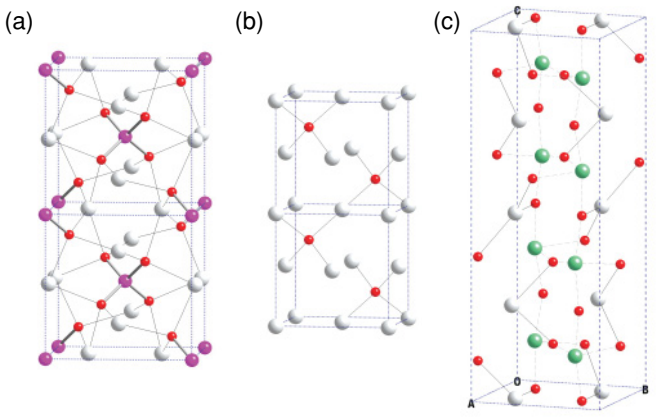

FIG. 1. (Color) Crystal structures for (a) Ag_3PO_4, (b) Ag_2O, and (c) $AgNbO_3$ where silver, red, magenta, and green particles denote Ag, O, P, and Nb atoms, respectively.

TABLE I. Lattice parameters computed for Ag_3PO_4, Ag_2O, and $AgNbO_3$ by LDA and LDA + U. U values are in eV.

Lattice parameters (Å)	Ag_3PO_4	Ag_2O	$AgNbO_3$
LDA	$a=5.90$	$a=4.66$	$a=5.48$ $b=5.58$ $c=15.49$
LDA + U	U(Ag) = 4.18 $a=5.88$	U(Ag) = 5.8 $a=4.67$	U(Ag) = 4.18, U(Nb) = 3.24 $a=5.48$ $b=5.57$ $c=15.66$
	U(Ag) = 9.75 $a=5.85$		U(Ag) = 9.75, U(Nb) = 7.56 $a=5.51$ $b=5.59$ $c=15.73$
Experiment	$a=6.00$[a]	$a=4.74$[b]	$a=5.5436$[c] $b=5.6071$[c] $c=15.565$[c]

[a]Reference 28.
[b]Reference 29.
[c]Reference 30.

TABLE II. Relaxed bond distances for Ag_3PO_4, Ag_2O, and $AgNbO_3$ given by LDA. The averaged values are shown for $AgNbO_3$. Experimental values are shown in parentheses.

Bond distance (Å)	Ag_3PO_4	Ag_2O	$AgNbO_3$
Ag-O	2.31 (2.36)[a]	2.02 (2.05)[b]	2.29 (2.41)[c]
Ag-Ag	2.95 (3.00)[a]	3.30 (3.35)[b]	3.90 (3.93)[c]
P-O	1.55 (1.56)[a]	...	...
Nb-O	...	...	2.01 (2.00)[a]

[a]Reference 28.
[b]Reference 29.
[c]Reference 30.

TABLE III. Band gaps for Ag_3PO_4, Ag_2O, and $AgNbO_3$ from LDA and LDA + U. The values of U are in eV. Ag_2O has a direct band gap at Γ, while Ag_3PO_4 has an indirect band gap from $M(1/2,1/2,0)$ to $\Gamma(0,0,0)$. $AgNbO_3$ also has an indirect band gap and its VBM depends on whether it is given by LDA or LDA + U [$(1/2,1/8,0)$ to $S(1/2,1/2,0)$ in LDA and $\Gamma(0,0,0)$ to $S(1/2,1/2,0)$ in LDA + U].

Band gap (eV)	Ag_3PO_4	Ag_2O	$AgNbO_3$
LDA	0.11	0.09	1.29
LDA + U	U(Ag) = 4.18	U(Ag) = 5.8	U(Ag) = 4.18, U(Nb) = 3.24
	0.65	0.17	1.61
	U(Ag) = 9.75		U(Ag) = 9.75, U(Nb) = 7.56
	1.30		2.25
Experiment	2.45[a]	1.3[b]	3.0[c]

[a]Reference 21.
[b]Reference 17.
[c]Reference 27.

Nb-O bonds are much shorter than Ag-O bonds in $AgNbO_3$, and Ag-Ag distances are very large as compared to those in Ag_3PO_4 and Ag_2O. Computational band gaps were 0.11, 0.09, and 1.29 eV for Ag_3PO_4, Ag_2O, and $AgNbO_3$, respectively, which underestimated the experimental results [2.45 eV,[21] 1.3 eV,[17] and 3.0 eV (Ref. 27)] owing to the common problem of LDA. Thus, we applied scissor operators of 2.34, 1.21, and 1.71 eV to Ag_3PO_4, Ag_2O, and $AgNbO_3$, respectively, for the sake of band-gap correction. Although the band gaps are slightly opened by the application of U to the d states, the underestimation was still observed in LDA + U. The results for the band gaps are summarized in Table III.

III. RESULTS AND DISCUSSIONS

Figures 2(a)–2(c) show DOS obtained from LDA with the band-gap correction for Ag_3PO_4, Ag_2O, and $AgNbO_3$, respectively. Here, k points are sampled at $13 \times 13 \times 13$, $19 \times 19 \times 19$, and $5 \times 5 \times 3$ for Ag_3PO_4, Ag_2O, and $AgNbO_3$, respectively. As shown in the insets of Figs. 2(a) and 2(b), the CBM mainly consists of Ag s states in Ag_3PO_4, while Ag d states predominate the CBM in Ag_2O. The significant difference is attributed to the formation of strongly covalent P-O bonds, which is evidenced in the local DOS for O sp and P sp in Fig. 2(a) as bonding states located at approximately −9 eV below the VBM. The partial charge density corresponding to one of these bonding states shown in Fig. 2(a) indicates the formation of a rigid tetrahedral unit of PO_4. This increases

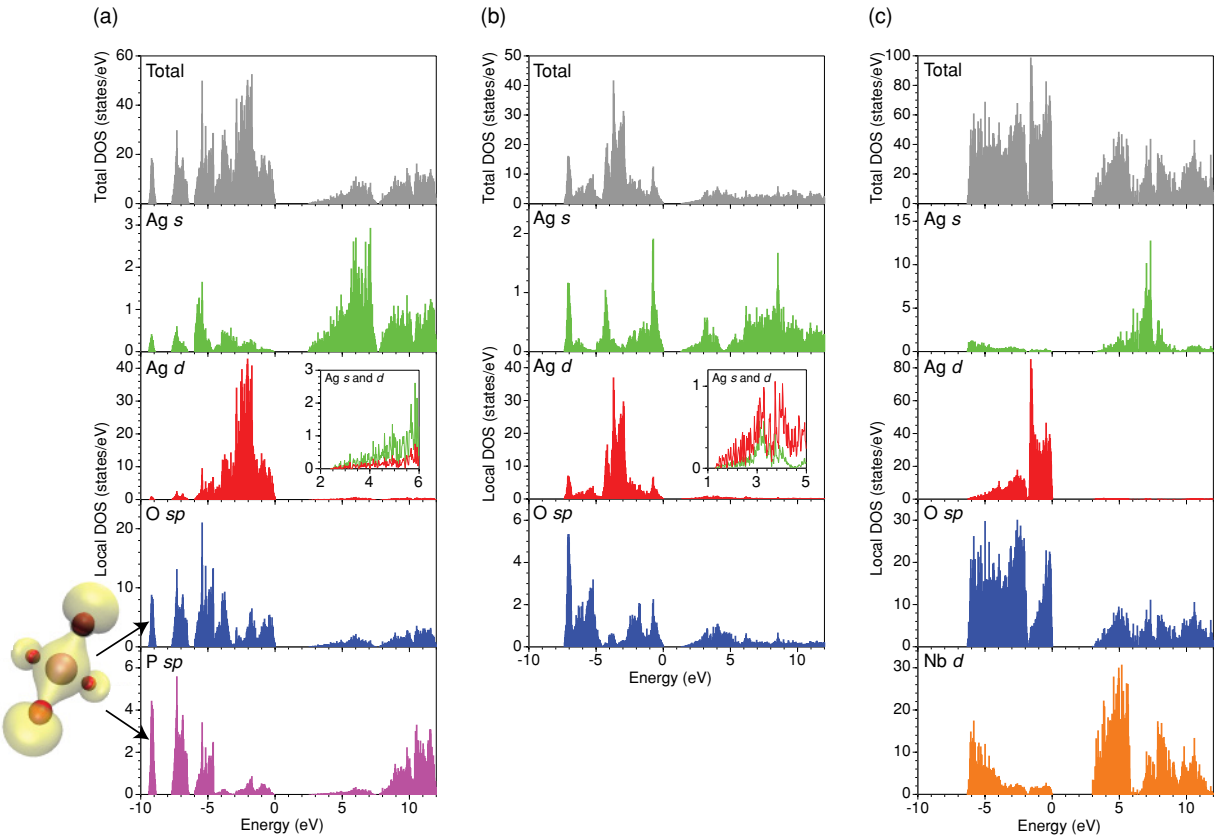

FIG. 2. (Color) Total and local DOS for (a) Ag_3PO_4, (b) Ag_2O, and (c) $AgNbO_3$. For the local DOS, we use spheres of radii 1.503, 0.82, 1.233, and 1.503 Å for Ag, O, P, and Nb, respectively. The zero energy is at the VBM. The insets in (a) and (b) show extended plots of DOS for Ag s and d at the energy range near the CBM. The partial charge density corresponding to one of the P-O bonding states is depicted in the leftmost area in (a). Here, the red and mauve particles denote the positions of O and P atoms, and the isosurface (yellow surface) is at 0.03 $e/Å^3$.

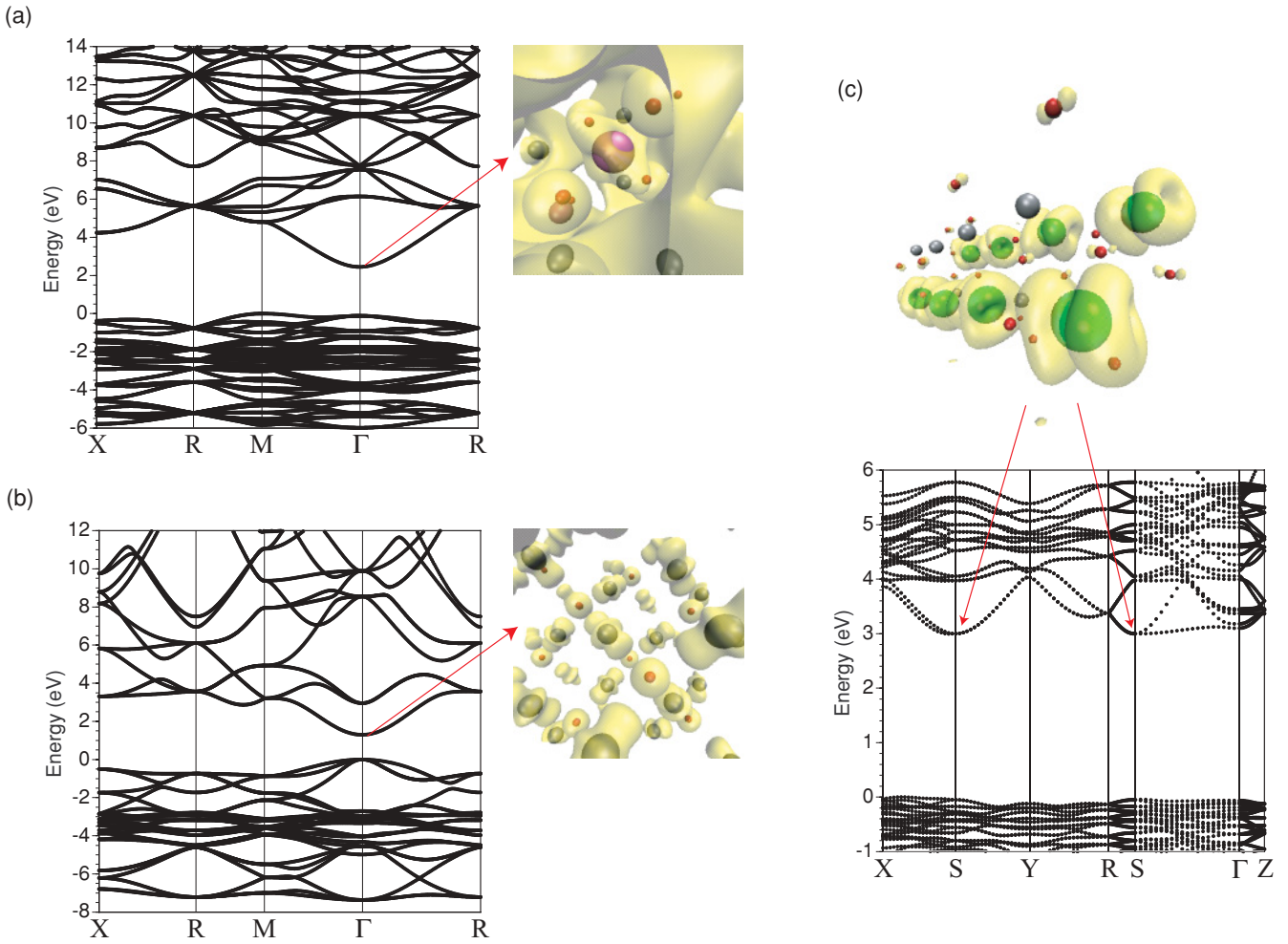

FIG. 3. (Color) Band structures for (a) Ag_3PO_4, (b) Ag_2O, and (c) $AgNbO_3$. The square of the wave function (yellow surface) corresponding to the CBM is also shown in each case, where silver, red, mauve, and green particles represent the positions of Ag, O, P, and Nb atoms, respecrively. The isosurfaces are at 0.01 $e/Å^3$.

the ionic character of Ag^+ and $(PO_4)^{3-}$, weakening the covalent nature of the Ag-O bonds. Thus, hybridization of Ag *d* and O *p* states is negligible in Ag_3PO_4, rendering fully occupied *d* states in the VBM. The weak Ag-O bonds are also reflected in the local DOS of Ag *d* in Fig. 2(a), in which no clear splitting into *d*-t_2 and *d*-*e* by tetrahedral crystal fields at the fourfold Ag was observed.[14] In contrast, Ag-O bonds are essentially formed in Ag_2O, and the appearance of *d* states in the CBM as Ag *d*-O *p* antibonding states is inevitable. Ag *s* states also hybridize with O *p* states, yet the antibonding states of Ag *s*-O *p* bonds are energetically higher than those of Ag *d*-O *p* bonds on average, and thus Ag *s* cannot become the predominant character of the CBM in Ag_2O. In $AgNbO_3$, the majority of the CBM is Nb *d* states [Fig. 2(c)] and the nature of Ag-O does not significantly affect the characteristic of the CBM.

In Figs. 3(a)–3(c), the band structures of Ag_3PO_4, Ag_2O, and $AgNbO_3$ are shown, respectively, with the square of the wave function corresponding to the CBM. In Ag_3PO_4, the wave function at the CBM, which mainly consists of Ag *s*, is well delocalized, resembling the charge distribution of metallic materials. In contrast, the CBM of Ag_2O possesses the character of Ag *d*-O *p* antibonding states. The difference originates from the absence of *d* states at the CBM of Ag_3PO_4, as discussed before. The *d* states are usually localized even under the formation of covalent bonds with oxygen, and thus the presence of *d* states at the CBM as in the case of Ag_2O [Fig. 3(b)] is disadvantageous for the electron transfer. In Ag_3PO_4, a large amount of hybridization between Ag *s* and Ag *s* occurs, as evidenced in the shorter distance of Ag-Ag bonds in Ag_3PO_4 than in Ag_2O (Table II), and this gives rise to the dispersive band structure at CBM without the "contamination" of *d* states. This contributes to a decreasing effective mass of the electron, as discussed below. The indirect band gap of Ag_3PO_4 (from *M* to Γ) might be beneficial also for the carrier separation, but this alone does not explain the exceptionally high performance of Ag_3PO_4 because most of the silver-based photocatalysts possess indirect band gaps.[13,14]

In $AgNbO_3$, the CBM consists mainly of d_{xz} and d_{yz}, showing an anisotropic charge distribution [Fig. 3(c)], allowing electron transfer only along the *z* direction. The anisotropy is also observed in the band structure, where the dispersion of the CBM depends strongly on the direction; it is very dispersive along $X-S-Y$, while it is very flat along $S-\Gamma$. This is undesirable for photocatalysis use because the limited orientation of

TABLE IV. Effective masses of the electron (m_e^*) and the hole (m_h^*) in the unit of free-electron mass for Ag_3PO_4 obtained from parabolic fitting to the CBM and the VBM along each direction in the reciprocal space, respectively. The three values of m_h^* correspond to three degenerate states at the VBM of Γ.

Direction	LDA	LDA + U	
		Γ:k = (0,0,0)	
		U(Ag) = 4.18	U(Ag) = 9.75
	m_e^*	m_e^*	m_e^*
(100)	0.41	0.41	0.41
(110)	0.42	0.42	0.42
(111)	0.43	0.42	0.42

Direction	LDA			LDA + U					
				Γ:k = (0,0,0)					
				U(Ag) = 4.18			U(Ag) = 9.75		
	$m_h^{(1)*}$	$m_h^{(2)*}$	$m_h^{(3)*}$	$m_h^{(1)*}$	$m_h^{(2)*}$	$m_h^{(3)*}$	$m_h^{(1)*}$	$m_h^{(2)*}$	$m_h^{(3)*}$
(100)	3.04	1.10	1.10	3.30	1.01	1.01	3.48	1.01	1.01
(110)	2.56	1.27	1.09	2.77	1.15	1.01	3.19	1.11	1.02
(111)	1.99	1.23	1.23	2.20	1.12	1.12	2.63	1.10	1.10
				M:k = (1/2,1/2,0)					
				U(Ag) = 4.18	U(Ag) = 9.75				
		m_h^*		m_h^*	m_h^*				
(100)		1.92		1.74	1.73				
(110)		2.08		1.88	1.88				
(111)		1.53		1.42	1.45				
(001)		1.04		0.99	1.03				

the electron transfer increases the possibility of encountering holes, causing carrier recombination. This also indicates that the $AgNbO_3$ (001) surface is especially active for reduction reactions because photoexcited electrons are transported along the (001) direction toward the surface. In most cases, however, photocatalysts are used in the form of a powder rather than as a thin film, and the selective nature of the reactive face is disadvantageous for photocatalysis applications. In contrast, the CBM of Ag_3PO_4 shows a very isotropic distribution because it mainly consists of spherically symmetric Ag s states, hybridized with other Ag s states, forming a highly delocalized wave function [Fig. 3(a)]. This suggests strongly that photocatalytic activities of Ag_3PO_4 do not significantly depend on the surface orientation, giving a clear explanation for the high performance of Ag_3PO_4 in powder form.[21] In fact, the efficiency of O_2 evolution from Ag_3PO_4 (636 μM/h) is much higher than that from $AgNbO_3$ (37 μM/h).

To validate the above picture, we have estimated the effective masses of the electron (m_e^*) and the hole (m_h^*) in Ag_3PO_4, Ag_2O, and $AgNbO_3$ by fitting parabolic functions to the CBM [Γ(0,0,0) for Ag_3PO_4 and Ag_2O, and S(1/2,1/2,0) for $AgNbO_3$] and the VBM at several k points along various directions in reciprocal space. The results given by LDA and LDA + U are summarized in Tables IV–VI. m_e^* is much smaller in Ag_3PO_4 ($\sim 0.4m_e$) than in Ag_2O ($\sim 0.6m_e$) in the case of LDA, where m_e is the free-electron mass. The relatively small m_e^* in Ag_3PO_4 reflects the dispersive band structure at the CBM [Fig. 3(a)]. The obtained value $\sim 0.4m_e$ for Ag_3PO_4 is comparable to m_e^* of indium tin oxide,[31] i.e., the widely used transparent conductive oxide, and much smaller than that of TiO_2 [$\sim 1m_e$ (Ref. 32)]. Moreover, m_e^* is small in every direction in Ag_3PO_4, reflecting the isotropic nature of the s

TABLE V. Effective masses of the electron (m_e^*) and the hole (m_h^*) in the unit of free-electron mass for Ag_2O obtained from parabolic fitting to the CBM and the VBM along each direction in the reciprocal space, respectively. The three values of m_h^* correspond to three degenerate states at the VBM of Γ.

Direction	LDA	LDA + U
	Γ:k = (0,0,0)	
		U(Ag) = 5.8
	m_e^*	m_e^*
(100)	0.61	0.47
(110)	0.61	0.47
(111)	0.62	0.47

Direction	LDA			LDA + U		
	Γ:k = (0,0,0)					
				U(Ag) = 5.8		
	$m_h^{(1)*}$	$m_h^{(2)*}$	$m_h^{(3)*}$	$m_h^{(1)*}$	$m_h^{(2)*}$	$m_h^{(3)*}$
(100)	2.06	2.06	0.17	2.34	2.34	0.23
(110)	2.09	0.55	0.23	2.34	0.72	0.32
(111)	1.82	0.33	0.33	1.94	0.45	0.45

TABLE VI. Effective masses of the electron (m_e^*) and hole (m_h^*) in the unit of free-electron mass for $AgNbO_3$ obtained from parabolic fitting to the CBM and the VBM along each direction in the reciprocal space, respectively. The two values of m_e^* correspond to two degenerate states at the CBM of $S(1/2,1/2,0)$.

Direction	LDA		LDA + U			
			S:$k=(1/2,1/2,0)$ $U(\mathrm{Ag})=4.18$ $U(\mathrm{Nb})=3.24$		$U(\mathrm{Ag})=9.75$ $U(\mathrm{Nb})=7.56$	
	$m_e^{(1)*}$	$m_e^{(2)*}$	$m_e^{(1)*}$	$m_e^{(2)*}$	$m_e^{(1)*}$	$m_e^{(2)*}$
(100)	0.79	0.79	0.67	0.67	0.77	0.77
(010)	0.88	0.68	0.72	0.61	0.80	0.74
(001)	0.35	0.35	0.33	0.33	0.39	0.39
(110)	7.60	0.46	7.16	0.36	10.03	0.42
(111)	3.45	0.46	3.35	0.37	4.18	0.43

Direction	LDA	LDA + U	
	$k=(1/2,1/8,0)$	Γ:$k=(0,0,0)$ $U(\mathrm{Ag})=4.18$ $U(\mathrm{Nb})=3.24$	$U(\mathrm{Ag})=9.75$ $U(\mathrm{Nb})=7.56$
	m_h^*	m_h^*	m_h^*
(100)	7.01	4.77	2.46
(010)	3.54	4.03	3.32
(001)	2.75	4.85	5.20
(110)	4.85	3.81	3.84
(111)	4.84	3.92	3.89

character. We found that the introduction of Hubbard U does not significantly affect the m_e^* of Ag_3PO_4 (Table IV) while a sizable change was observed in the m_e^* of Ag_2O (Table V). The decrease of m_e^* from $\sim 0.6m_e$ (LDA) to $\sim 0.47m_e$ (LDA + U) in Ag_2O is interpreted as the weakened hybridization of Ag d and O p owing to the effect of U, which localizes the d states. The s character is, therefore, enhanced at the CBM, leading to the smaller value of m_e^* in LDA + U. In Ag_3PO_4, however, Ag-O bonds are originally weakened in the LDA level thanks to the formation of the strong P-O bonds, and the effect of localizing Ag d states does not affect the value of m_e^*. It is interesting to note that the effective mass of hole m_h^* exhibits a rather opposite trend to m_e^*. We found that m_h^* at Γ is greater in Ag_3PO_4 than in Ag_2O, on average. This must be the result of the higher density of d states at the valence band in Ag_3PO_4 (Fig. 2), leading to a less dispersive band structure. In other words, the hybridization of Ag d and O p owing to the strong Ag-O bonds in Ag_2O increases dispersion of the VBM. The large difference in m_e^* and m_h^* might be relevant to the suppression of the carrier recombination in Ag_3PO_4, yet more detailed studies for the carrier recombination mechanism is required to conclude this point. m_h^* is somewhat smaller at M than at Γ in Ag_3PO_4, and thus the hole transfer should be encouraged in a condition where the indirect photoexcitation from M to Γ is promoted. This might be realized by increasing the temperature for activating phonon vibrations. In $AgNbO_3$, m_e^* widely ranges from $0.35m_e$ to $7.60m_e$, strongly depending on the direction (Table VI). Here, m_e^* is smallest along (001), reflecting the anisotropic distribution of the wave function at the CBM of $AgNbO_3$ [Fig. 3(c)]. The anisotropic nature of m_e^* remains unchanged in LDA + U. Contrary to the case in Ag_2O, the introduction of the Hubbard U is unable to decrease m_e^* in $AgNbO_3$. This is because Ag s-Ag s hybridization is limited in $AgNbO_3$ owing to the long Ag-Ag distances (Table II), and the majority of Ag s states locate at a relatively higher position in the conduction band [Fig. 2(c)]. Thus, an upward shift of the unoccupied Nb d states upon the application of U does not help the increasing Ag s character at the CBM. On the other hand, the application of U to Ag d and Nb d significantly affects the absolute values of m_h^*. First of all, the k point associated with the VBM is altered by the introduction of U from $(1/2,1/8,0)$ to $(0,0,0)$. The on-site Coulomb repulsion shifts the occupied d states downward, leaving O sp states at the VBM. Because the valence band of $AgNbO_3$ is relatively flat, as shown in Fig. 3(c), the position of the k point, which gives the maximum value of the valence band, is sensitive to the change of the band character. For the same reason, m_h^* is smaller as U increases (Table VI), i.e., the d character is swept out of the VBM, enhancing the band dispersion.

In Ag_3PO_4, electrons are rapidly transferred to the surface because of their small effective mass along every direction, thanks to the wide dispersion of the CBM originating from Ag s character. As a result, excited electrons are efficiently scavenged by sacrificial reagents on the surface. The quick motion of electrons might prohibit the carrier recombination with hole carriers, although this point must be investigated carefully in the future. In most photocatalysts, including widely used TiO_2, however, the d state is one of the major components

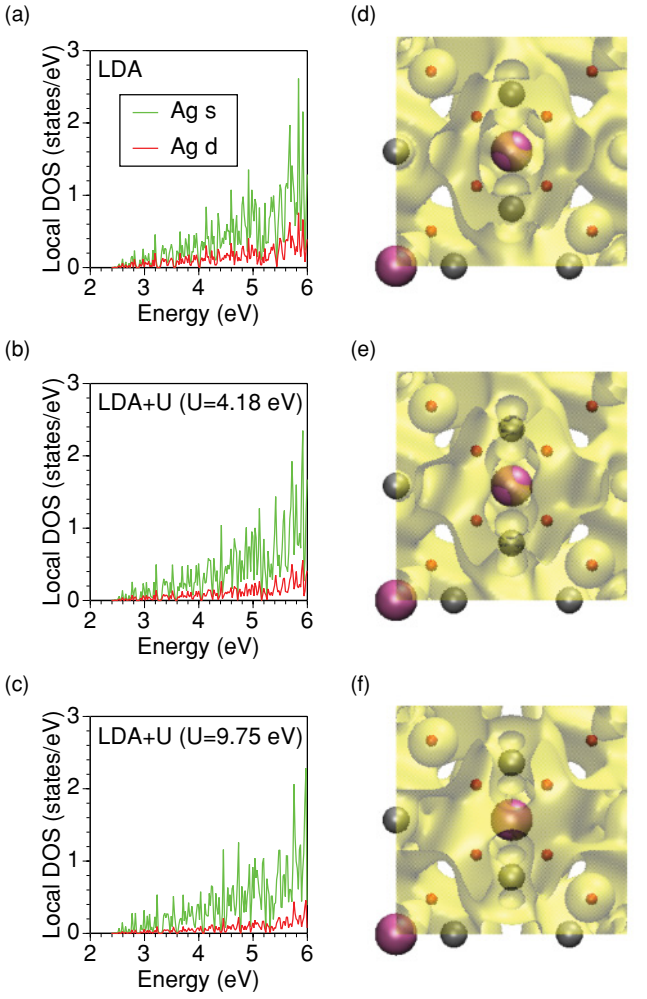

FIG. 4. (Color) Local DOS for Ag_3PO_4 projected onto Ag s and Ag d given by (a) LDA, (b) LDA + $U^{(1)}$ [U(Ag) = 4.18 eV], and (c) LDA + $U^{(2)}$ [U(Ag) = 9.75 eV]. The square of the wave functions corresponding to the CBM are also shown for (d) LDA, (e) LDA + $U^{(1)}$, and (f) LDA + $U^{(2)}$. The isosurfaces of the wave functions are at 0.01 $e/Å^3$. Silver, red, and mauve particles represent the positions of Ag, O, and P atoms, respectively.

of the CBM, and thus a high mobility of electrons cannot be expected. This explains the low quantum yield of most photocatalysts based on transition-metal oxides. In a neutral Ag atom ([Kr]$4d^{10}5s^1$), d states are occupied as valence, and the ionic nature of $3Ag^+ + (PO_4)^{3-}$ inhibits the appearance of the d states in the CBM, distinctly splitting the band character of the CBM (Ag s) from the VBM (Ag d + O p). The high performance of Ag_3PO_4 as a photocatalyst is, therefore, attributed to the absence of the d character in the CBM.

Our finding suggests a useful strategy for designing photocatalytic materials: One must get rid of the d states from the CBM so as to decrease m_e^* and enhance carrier separations. This must be achieved by introducing p-block elements with electronegativity closer to that of oxygen into an oxide MO_x, where M is a transition metal with d^{10} and partially occupied s states. Such p-block elements can form strongly covalent bonds with oxygen, weakening the covalent nature of the M-O bonds. This helps pulling the d states down to the VBM and

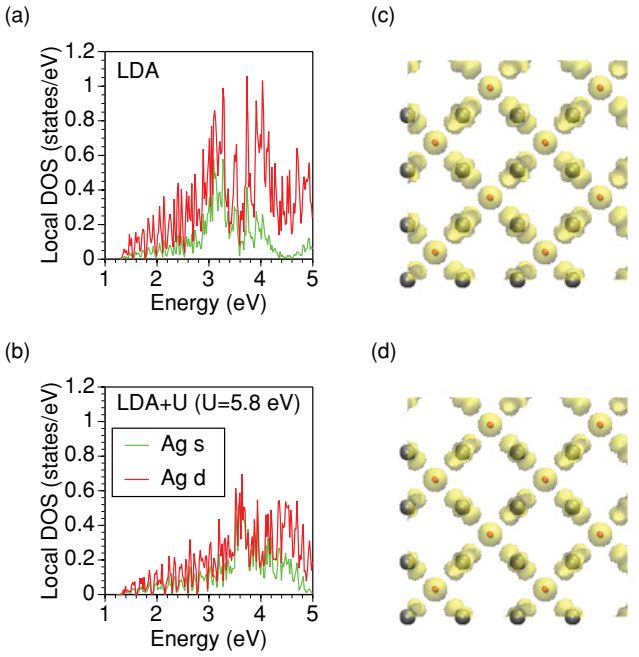

FIG. 5. (Color) Local DOS for Ag_2O projected onto Ag s and Ag d given by (a) LDA and (b) LDA + U [U(Ag) = 5.8 eV]. The square of the wave functions corresponding to the CBM are also shown for (c) LDA and (d) LDA + U. The isosurfaces of the wave functions are at 0.01 $e/Å^3$. Silver and red particles represent the positions of Ag and O atoms, respectively.

decreasing m_e^*, which promotes carrier transfer to the surface area.

It must be mentioned that photocatalytic reactions consist mainly of three processes: (1) photoexcitation of electron and holes, (2) carrier transfers to the surface area, and (3) chemical reactions on the surface. The present study is related to the first two processes, which are determined by bulk properties. Hence, it is still an open question whether the surface structure of Ag_3PO_4 is advantageous for the photocatalytic reactions. The answer to this question is out of the scope of this work and is left for future research.

Finally, we would like to emphasize that our conclusion is independent of the computational methods LDA and LDA + U. In Figs. 4(a)–4(f), the local DOS of Ag_3PO_4 projected onto Ag s and Ag d at the energy range near the CBM are compared for LDA and LDA + U with the wave function corresponding to the CBM. The overall trend, i.e., CBM consists of Ag s states and the wave function is highly delocalized, is the same among the three different calculations, LDA, LDA + $U^{(1)}$, and LDA + $U^{(2)}$. Similarly, Ag d states are found to be the predominant character at the CBM in Ag_2O and its wave function consists mainly of Ag-O antibonding states in LDA + U (Fig. 5), although the magnitude of Ag d states over Ag s is slightly decreased in LDA + U owing to the localization of Ag d states, as discussed earlier.

IV. CONCLUSIONS

We have studied the electronic structures of three different Ag-based oxides Ag_3PO_4, Ag_2O, and $AgNbO_3$ to understand the high photocatalytic performance of Ag_3PO_4. Our analysis

on the DOS and band structures has revealed that the CBM of Ag_3PO_4 consists mainly of Ag *s* states owing to the formation of the rigid tetrahedral units PO_4, which weaken and strengthen Ag-O and Ag-Ag bonds, respectively. This contributes to a very dispersive electronic structure at the CBM, leading to a highly delocalized and isotropic distribution of the wave function. In contrast, another photocatalyst, $AgNbO_3$, possesses a Nb *d* character at the CBM, showing an anisotropic distribution of the wave function. The difference in the electronic structures of these two photocatalysts is reflected in the effective mass of electrons; m_e^* is relatively small in every direction in Ag_3PO_4, and is thus advantageous for electron transfers, while it strongly depends on the direction in $AgNbO_3$. Therefore, we conclude that the excellent photocatalytic performance of Ag_3PO_4 is attributed partly to the highly dispersive band structure of the CBM resulting from Ag *s*-Ag *s* hybridization without localized *d* states.

ACKNOWLEDGMENTS

We would like to thank T. Kako, N. Kikugawa, T. Matsumoto, T. Ohno, F. Shimojo, A. Kudo, and M. Klein for useful discussions and advice. This work was supported by the Japan Society for the Promotion of Science KAKENHI (21760030).

[1] M. Kaneko and I. Okura, *Photocatalysis Science and Technology* (Springer, New York, 2002).
[2] A. L. Linsebigler, G. Lu, and J. T. Yates Jr., Chem. Rev. **95**, 735 (1995).
[3] M. R. Hoffmann, S. T. Martin, W. Choi, and D. W. Bahnemann, Chem. Rev. **95**, 69 (1995).
[4] A. Fujishima and K. Honda, Nature (London) **238**, 37 (1972).
[5] K. E. Karakitsou and X. E. Verykios, J. Phys. Chem. **97**, 1184 (1993).
[6] H. Yamashita, M. Harada, J. Misaka, M. Takeuchi, Y. Ichihashi, F. Goto, M. Ishida, T. Sasaki, and M. Anpo, J. Synchrotron Radiat. **8**, 569 (2001).
[7] R. Asahi, T. Morikawa, T. Ohwaki, K. Aoki, and Y. Taga, Science **293**, 269 (2001).
[8] H. Wang and P. Lewis, J. Phys.: Condens. Matter **18**, 421 (2006), and references therein.
[9] Z. Zou, J. Ye, K. Sayama, and H. Arakawa, Nature (London) **414**, 625 (2001).
[10] K. Maeda, K. Teramura, D. Lu, T. Takata, N. Saito, Y. Inoue, and K. Domen, Nature (London) **440**, 295 (2006).
[11] H. Kato, H. Kobayashi, and A. Kudo, J. Phys. Chem. B **106**, 12441 (2002).
[12] S. Ouyang, H. Zhang, D. Li, T. Yu, J. Ye, and Z. Zou, J. Phys. Chem. B **110**, 11677 (2006).
[13] Y. Maruyama, H. Irie, and K. Hashimoto, J. Phys. Chem. B **110**, 23274 (2006).
[14] S. Ouyang, N. Kikugawa, D. Chen, Z. Zou, and J. Ye, J. Phys. Chem. C **113**, 1560 (2009).
[15] X. Li, S. Ouyang, N. Kikugawa, and J. Ye, Appl. Catal., A **334**, 51 (2008).
[16] T. Kako, N. Kikugawa, and J. Ye, Catal. Today **131**, 197 (2008).
[17] L. H. Tjeng, M. B. J. Meinders, J. van Elp, J. Ghijsen, G. A. Sawatzky, and R. L. Johnson, Phys. Rev. B **41**, 3190 (1990).
[18] K. Ikarashi, J. Sato, H. Kobayashi, N. Saito, H. Nishiyama, and Y. Inoue, J. Phys. Chem. B **106**, 9048 (2002).
[19] N. Arai, N. Saito, H. Nishiyama, Y. Inoue, K. Domen, and K. Sato, Chem. Lett. **35**, 796 (2006).
[20] J. F. Wager, D. A. Keszler, and R. E. Presley, *Transparent Electronics* (Springer, New York, 2008).
[21] Z. Yi, J. Ye, N. Kikugawa, T. Kako, S. Ouyang, H. Stuart-Williams, H. Yang, J. Cao, W. Luo, Z. Li, Y. Liu, and R. L. Withers, Nat. Mater. **9**, 559 (2010).
[22] G. Kresse and J. Hafner, Phys. Rev. B **47**, 558 (1993).
[23] G. Kresse and J. Furthmüller, Phys. Rev. B **54**, 11169 (1996).
[24] V. I. Anisimov, F. Aryasetiawan, and A. I. Lichtenstein, J. Phys.: Condens. Matter **9**, 767 (1997).
[25] A. Janotti., D. Segev, and C. G. Van de Walle, Phys. Rev. B **74**, 045202 (2006).
[26] J. P. Perdew and A. Zunger, Phys. Rev. B **23**, 5048 (1981).
[27] M. Kruczek, E. Talik, and A. Kania, Solid State Comm. **137**, 469 (2006).
[28] R. W. G. Wyckoff, Am. J. Sci. **10**, 107 (1925).
[29] R. W. G. Wyckoff, *Crystal Structure*, Vol. 1 (Wiley, New York, 1965).
[30] P. Sciau, A. Kania, B. Dkhil, E. Suard, and A. Ratuszna, J. Phys.: Condens. Matter **16**, 2795 (2004).
[31] H. Fujiwara and M. Kondo, Phys. Rev. B **71**, 075109 (2005).
[32] D. Kurita, S. Ohta, K. Sugiura, H. Ohta, and K. Koumoto, J. Appl. Phys. **100**, 096105 (2006).